Stabilizing a 22 karat nanogolden cage

Q. Wang,[1] Q. Sun,[1,2] and P. Jena[1]
[1]*Department of Physics, Virginia Commonwealth University, Richmond, Virginia 23284, USA*
[2]*Department of Advanced Materials and Nanotechnology, Peking University, Beijing 1000871, China*

(Received 2 September 2009; accepted 29 October 2009; published online 23 November 2009)

Since the discovery of C_{60} fullerene, considerable efforts have been devoted to find other elements with similar hollow cage structures. However, search for hollow *metallic* cages with a diameter similar to that of C_{60} fullerene has been elusive. We describe a procedure for the rational design of metallic cages by suitably choosing their size, composition, and charge state. A 22 karat nanogolden cage with a diameter of about 8.5 Å and consisting of 12 Al and 20 Au atoms is found to be metastable, which can be stabilized by embedding a Mn_4 cluster. In contrast to bulk Mn, which is antiferromagnetic, and isolated Mn_4 cluster, which is ferromagnetic with a giant magnetic moment of $20\mu_B$, the $Mn_4@Al_{12}Au_{20}$ endohedral complex exhibits magnetic bistability with $0\mu_B$ and $14\mu_B$ configurations being energetically nearly degenerate. These results, based on density functional theory, open the door to design a novel class of endohedral complexes with possible applications. © *2009 American Institute of Physics*. [doi:10.1063/1.3266562]

I. INTRODUCTION

The discovery of C_{60} fullerene[1] as the third form of carbon has been one of the most exciting developments in nanoscience and technology in recent years. With a hollow cage structure and diameter of 6.83 Å, C_{60} can encapsulate other atoms or clusters. Since these endohedral complexes can have technological applications, numerous attempts have been made to find other elemental clusters that can form similar hollow cage structures. Boron, an element adjacent to carbon, has been found to exhibit cage[2] as well as tubular motifs.[3] However, metal clusters, due to their flexible bonding scheme, do not prefer hollow cage structures. Exception to this rule has been recently found in small Au (Ref. 4) and Sn (Ref. 5) clusters, which show evidence for hollow cage geometries, although over a very narrow size range. In particular, much attention has recently been focused on nano-Au due to its extraordinary physical and chemical properties. Unlike bulk gold, which is chemically inert and nonmagnetic, nanogold can be reactive[6] and magnetic.[7] Au clusters containing 2–20 atoms show a remarkable progression of structures. They form planar geometries up to 12 atoms and hollow cages between 14 and 18 atoms.[8] Au_{20} cluster assumes a compact tetrahedral form that mimics the Au (111) surface morphology.[9] Due to the small size of the Au cage structures, they are not capable of encapsulating a cluster or a large atom.

The question then remains: is it possible to construct large hollow cages of *metal* clusters by changing their size, composition, and charge state? Recently Kumar[10] found that when 20 Au atoms are coated on an Al_{13} cluster (one Au atom on each of the 20 triangular faces of the Al_{13} icosahedron), an endohedral cage structure having a nearly spherical shape with an Al atom at the center is formed. Removing the central atom and adding two electrons give rise to the $Al_{12}Au_{20}^{2-}$ cluster that has 58 electrons. This is enough to fill the $1s^21p^61d^{10}2s^21f^{14}2p^61g^{18}$ electronic shells of a jellium model cluster where the positive charges of the ion cores are uniformly distributed over the jellium sphere. In nearly free electron metals it has been found[11] that electronic shell closure leads to enhanced stability of clusters, which manifest as conspicuous peaks in the mass spectra. These clusters commonly referred to as magic clusters can serve as building blocks of a novel class of cluster assembled materials.[12] The finding that $Al_{12}Au_{20}^{2-}$ cluster has a hollow cage structure while Au_{32} containing the same number of atoms does not[13] raises some interesting questions and possibilities. The question is whether this cage structure is the most stable configuration or it belongs to a local minimum in the potential energy landscape. This is particularly pertinent as the diameter of the $Al_{12}Au_{20}^{2-}$ cluster is large, namely, about 8.5 Å. If the hollow cage is indeed the preferred structure, the space in its interior may be large enough to accommodate another cluster. The possibility that a hollow metallic cage can be synthesized by varying its size, composition, and charge can thus lead to the rational design of a new class of endohedral complexes.

Using density functional theory and molecular dynamics (MD) simulation, we have examined a series of isomers of $Al_{12}Au_{20}$, $Al_{12}Au_{20}^{-}$, and $Al_{12}Au_{20}^{2-}$ clusters and found that hollow cage structures of all these clusters are *not* the lowest energy structures. The structures where four of the Au atoms form an endohedral core lie lower in energy. However, we have found two hollow cage structures of $Al_{12}Au_{20}^{2-}$ cluster with I_h and T_h symmetries that are metastable as all normal mode frequencies are positive. In addition, MD simulations at temperatures of up to 300 K do not show any structural transition. We examined the possibility that these metastable hollow cages can be further stabilized by embedding another small cluster. We used Mn_4 cluster as a test system. The choice of Mn was dictated by its unique properties from atomic to bulk phase. A Mn atom, due to its half filled $3d$ and filled $4s$ shells ($3d^54s^2$), interacts weakly, and bulk Mn has the lowest cohesive energy of any $3d$ transition metal sys-

tem. The magnetic moment of Mn atom is $5\mu_B$ and small clusters of Mn containing three to five atoms couple ferromagnetically, while bulk Mn is antiferromagnetic. Mn_4 carries a giant magnetic moment of $20\mu_B$,[14] which is retained even when it is embedded in a rare gas matrix.[15] Can Mn_4 retain its magnetic moment when embedded inside a metallic cage such as $Al_{12}Au_{20}^{2-}$ cluster?

In this paper we show that $Mn_4@Al_{12}Au_{20}^{2-}$ cluster is stable and has a binding energy of 5.29 eV against dissociation into Mn_4 and $Al_{12}Au_{20}^{2-}$. In addition, the endohedral complex exhibits magnetic bistability with $0\mu_B$ and $14\mu_B$ configurations being energetically nearly degenerate. The stability of the dianionic cluster suggests that the negative charges can be counterbalanced by incorporating appropriate cations and the resulting ionically bonded complex (e.g., $Cs_2Mn_4@Al_{12}Au_{20}$) can form the building block of a new salt where the magnetic bistability of the anion complex can be manipulated to fabricate new magnetic devices. In the following we discuss our numerical procedure and results.

The calculations were carried out by using density functional theory and generalized gradient approximation using the Perdew-Wang 91 functional.[16] A plane-wave basis set and the projector augmented wave potentials[17] with the valence states $5d^{10}6s^1$ for Au, $3s^2p^1$ for Al, and $3p^63d^54s^2$ for Mn, as implemented in the Vienna *ab initio* simulation package (VASP) (Ref. 18) were employed. The geometries were optimized without any symmetry constraint by starting with several initial configurations. High precision calculations with a cutoff energy of 450 eV for the plane-wave basis were performed. We used a supercell approach where the clusters were placed at the center of a $26\times26\times26$ Å^3 cubic cell. Due to the large supercell, the Brillouin zone integration was carried out only at the Γ point. In all calculations, self-consistency was achieved with a tolerance in the total energy of at least 0.3 meV. Hellmann–Feynman force components on each ion in the supercell were converged to 1 meV/Å. In order to check the thermal stability of the cage structures, we have carried out constant temperature MD simulations at 300 K with 0.5 fs time steps. The canonical ensemble was simulated by means of a Nosé thermostat[19] as implemented in the VASP package.

In the first row of Fig. 1 we provide the starting geometries of four isomers (labeled A, B, C, and D) of the $Al_{12}Au_{20}$ cluster. The first isomer (A) chosen by Kumar[10] has icosahedral symmetry (I_h) where 12 Al atoms occupy the vertices of an icosahedron and 20 Au atoms were placed above the center of its 20 triangular faces. This structure was chosen since Al_{13} is known to be an icosahedron. Isomer B consists of a Au_{20} core, which was coated with 12 Al atoms. Note that Au_{20} cluster is known to be very stable and has a tetrahedral symmetry. Each of the four faces of this tetrahedron can be decorated with three Al atoms, which lie above each of the rhombus structure formed by four Au atoms. This isomer has T_h symmetry and is dominated by Au–Au bonds. The third isomer C is another hollow cage belonging to the T_h symmetry group where the surface is marked by rectangular and hexagonal faces as opposed to pentagonal faces in isomer A. The fourth isomer D has T symmetry where four of the Au atoms in isomer A are pushed into the cage to form an endohedral complex. In the following we discuss the geometries and relative stabilities of the four isomers for different charge states.

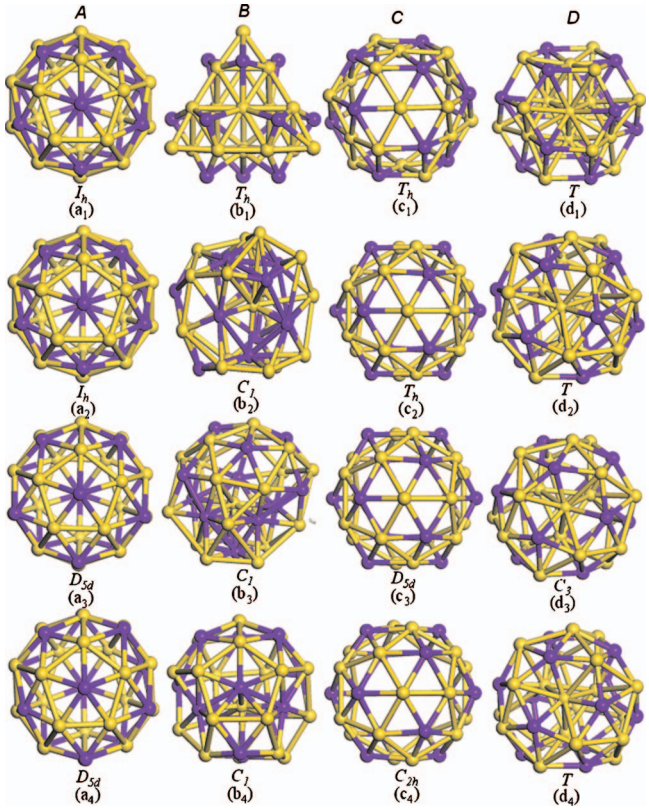

FIG. 1. A–D represent starting structures of four isomers of $Al_{12}Au_{20}$. Optimized geometries and their corresponding symmetries in dianionic, anionic, and neutral states are given in (a_2)–(d_2), (a_3)–(d_3), and (a_4)–(d_4), respectively.

II. DIANIONIC $Al_{12}Au_{20}^{2-}$ CLUSTERS

We first discuss the stability of various isomers of $Al_{12}Au_{20}^{2-}$ cluster. We recall that the number of valence electrons responsible for the bonding of $Al_{12}Au_{20}^{2-}$ cluster is 58 of which 36 valence electrons are contributed by 12 Al atoms and 20 valence electrons are contributed by 20 Au atoms. With the added two electrons $Al_{12}Au_{20}^{2-}$ cluster has enough to fill the $1s^21p^61d^{10}2s^21f^{14}2p^61g^{18}$ electronic shells of an otherwise jellium cluster. Clusters with electronically closed shells tend to have higher symmetry and are more stable than their adjoining neighbors. Optimized structures of $Al_{12}Au_{20}^{2-}$ cluster resulting from the four starting configurations are shown in Figs. $1(a_2)$–$1(d_2)$. The relative energies of these isomers measured with respect to the lowest energy structure are given in Table I. The lowest energy structure of this dianion is that of an endohedral structure where a Au_4 tetrahedron is encapsulated by 12 Al and 16 Au atoms [Fig. $1(d_2)$]. It lies 0.419 eV lower in energy than the structure identified by Kumar[10] as the preferred energy structure [see Fig. $1(a_2)$]. The hollow cage structure originating from isomer C with T_h symmetry is nearly degenerate with the one having I_h symmetry in Fig. $1(a_2)$. Optimization of isomer B in Fig. $1(b_1)$ initially led to a structure that was found to be 4.021 eV higher in energy than the lowest energy structure in

TABLE I. Relative energies $\Delta\varepsilon$ (in eV) calculated with respect to the lowest energy configuration, the HOMO-LUMO gaps Δ_{gap} (in eV), and the average Al–Au and Au–Au bond lengths (in angstrom) for each isomer of $Al_{12}Au_{20}$ in different charge states. See Fig. 1 for corresponding geometries. The energy costs to remove an electron from $Al_{12}Au_{20}^{2-}$ are 2.438, 2.725, 2.591, and 2.735 eV, respectively, for the four isomers in Figs. 1(a$_2$)–1(d$_2$), and those from $Al_{12}Au_{20}^{-}$ are 3.382, 3.643, 3.373, and 3.715 eV [see Figs. 1(a$_3$)–1(d$_3$)].

Al_2Au_{20}	Dianion				Anion				Neutral			
Isomers	A	B	C	D	A	B	C	D	A	B	C	D
$\Delta\varepsilon$	0.419	0.772	0.411	0.00	0.161	0.868	0.165	0.000	0.254	0.00	0.362	0.563
Δ_{gap}	0.407	0.418	0.452	1.150	0.176	0.092	0.161	0.101	0.200	0.134	0.214	0.110
d_{Al-Au}	2.607	2.545	2.613	2.600	2.605	2.546	2.605	2.600	2.599	2.547	2.600	2.600
d_{Au-Au}	2.821	2.851	2.823	2.877	2.810	2.842	2.810	2.876	2.804	2.835	2.808	2.877

Fig. 1(d$_2$). A close examination showed that this structure was dominated with more Au–Au bonds than any of the isomers in Figs. 1(a$_2$), 1(c$_2$), and 1(d$_2$). This is a direct consequence of the fact that the starting configuration (isomer B) also had a large number of Au–Au bonds due to the pyramidal structure of the Au_{20} cluster. In order to see if this structure corresponds to a local minimum, we carried out MD simulation at 300 K for 5000 time steps with each time step lasting for 0.5 fs. The structure at the end of the simulation was then reoptimized at 0 K. The resulting geometry is shown in Fig. 1(b$_2$). It is 0.772 eV higher in energy than the lowest energy structure in Fig. 1(d$_2$). Note that Fig. 1(b$_2$) is no longer dominated by Au–Au bonds. We also note from Table I that the highest occupied molecular orbital and the lowest unoccupied molecular orbital (HOMO-LUMO) gap of the lowest energy endohedral complex is 1.150 eV, which further confirms its enhanced stability.

We note that in all the isomers, there are no Al–Al bonds; only Al–Au and Au–Au bonds exist. This is consistent with the binding energies of Al_2, Au_2, and AlAu dimers, which are respectively 1.380, 2.350, and 3.390 eV.[20] The stronger Au–Au and Al–Au bonds ensure that in a stable structure number of these bonds are maximized. The average bond lengths between Al–Au and Au–Au in all the isomers are not same (see Table I). The structure originating from isomer B has a shorter average Al–Au bond length (2.545 Å), corresponding to its compact configuration, while the structure in Fig. 1(d$_2$) has a longer average Au–Au bond length of 2.877 Å. We note that all these bond lengths are larger than those of their respective dimers, namely, 2.339 Å for AlAu dimer[21] and 2.472 Å for Au_2 dimer.[22]

Although the hollow cage structures of $Al_{12}Au_{20}^{2-}$ cluster in Figs. 1(a$_2$) and 1(c$_2$) are not the energetically most favorable cluster, we discuss their properties further because they both have a diameter of about 8.5 Å. Since this is much larger than the diameter of C_{60} (6.83 Å), $Al_{12}Au_{20}^{2-}$ cluster can accommodate another cluster inside its hollow cage. To establish the stability of cage structures further, we first confirmed that all their normal mode frequencies are positive, indicating that the cages belong to a local minimum in the potential energy surface. We then carried out MD simulations at elevated temperatures. The clusters were heated to 300 K, allowed to equilibrate over 5000 time steps, and then reoptimized at 0 K. The resulting geometries remain as a cage with initial symmetries intact but with minor fluctuations in bond lengths. For example, in Fig. 1(a$_2$) Al–Au bond length increased by 0.23%, while Au–Au bond length decreased by −0.16%. This supports our conclusion that the hollow cage structures are metastable. The HOMO-LUMO gap of the structure in Fig. 1(a$_2$) is calculated to be 0.407 eV, in good agreement with Kumar's result.[10] The HOMO is dominated by the orbitals of Al atoms [see Fig. 2(a)], while the LUMO is from the orbitals of both Al and Au sites. The deformation density for the cage structure of $Al_{12}Au_{20}^{2-}$ cluster is plotted in Fig. 2(b), which shows some covalent character in the Al–Au bonds. We note that the diameter of the cage measured with respect to Al–Al distance is 8.393 Å, while that measured with respect to Au–Au distance is 7.840 Å. Hence, the cage is nearly spherical.

III. ANIONIC $Al_{12}Au_{20}^{-}$ CLUSTERS

We further examined the stability of $Al_{12}Au_{20}^{2-}$ cluster against autodetachment of an electron. To this end we removed one electron from each of the four isomers of $Al_{12}Au_{20}^{2-}$ cluster and reoptimized the geometries. The results are given in Figs. 1(a$_3$)–1(d$_3$). Note that the symmetry of most of the isomers changed as an electron is removed from the dianion. For instance, the symmetry of the lowest energy structure of the anion changed from T to C_3 [see Figs. 1(d$_2$) and 1(d$_3$)]. Two of the hollow cage isomers resulting from the optimization of the first and third isomer in Figs. 1(a$_2$)–1(c$_2$) are energetically nearly degenerate and lie about 0.16 eV above the lowest energy structure, while that resulting from isomer in Fig. 1(b$_2$) lies 0.868 eV higher in energy.

The energy cost to remove an electron from the $Al_{12}Au_{20}^{2-}$ cluster varies between 2.44 and 2.74 eV for the

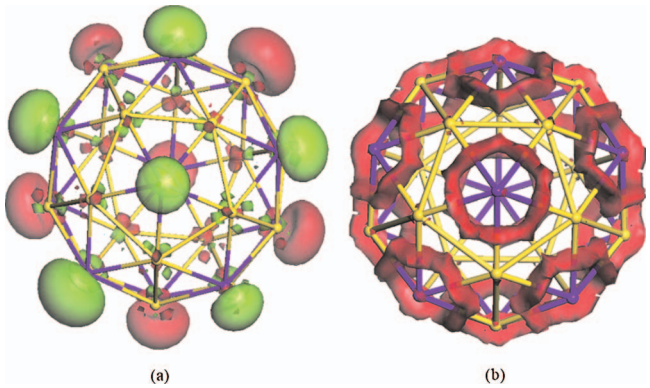

FIG. 2. Isosurfaces of the HOMO (0.035 $e/Å^3$) and (b) the deformation density (0.035 $e/Å^3$) for the I_h cage structure of $Al_{12}Au_{20}^{2-}$ cluster.

four isomers with the endohedral cage structure [Fig. 1(d_3)] being the most stable isomer against autoelectron detachment. The average Al–Au and Au–Au bond lengths in $Al_{12}Au_{20}^{2-}$ clusters, however, remain essentially unchanged from that in the dianion. These results, shown in Table I, further confirm the stability of the dianion, which arises due to the filling of the electronic shells.

IV. NEUTRAL $Al_{12}Au_{20}$ CLUSTERS

The structure and relative stability of neutral $Al_{12}Au_{20}$ cluster are examined by removing an electron from the anion and reoptimizing the geometries for all the four isomers. The adiabatic electron affinity calculated by taking the energy difference between the optimized anion and corresponding neutral clusters can be compared with values obtained from photoelectron spectroscopy (PES) experiments when available. The optimized geometries of the neutral isomers are given in Figs. 1(a_4)–1(d_4). Note that the lowest energy structure with symmetry C_1 [Fig. 1(b_4)] results from isomer B. The relative energies of the isomers of the neutral complex measured with respect to this lowest energy configuration are given in Table I. We note that the symmetry of the neutral cage isomer is lowered from that of its dianion due to Jahn–Teller effect. Correspondingly, the HOMO-LUMO gap is also reduced. The adiabatic electron affinity of the lowest energy structure in Fig. 1(b_4) is 3.643 eV. The electron affinities of structures derived from isomers A and C are nearly the same, namely, about 3.4 eV, while that derived from isomer D is 3.715 eV. Since the lowest energy structures of the neutral and anionic $Al_{12}A_{20}$ clusters are different (the former has C_1 symmetry, while the later has C_3 symmetry), the peaks in the PES should be broad unless an energy barrier separates the two structures. Thus, it will be illuminating to have PES experiments performed on these clusters.

V. Mn_4 ENCAPSULATED IN $Al_{12}Au_{20}$ CAGE

The existence of metastable hollow cages of $Al_{12}Au_{20}^{2-}$ cluster along with the observation that their lower energy isomer has an Au_4 tetrahedron embedded inside shows that the cage is large enough to accommodate small clusters. To explore this possibility we concentrated on a Mn_4 cluster as an endohedral complex because of its unique magnetic properties. Note that bulk Mn is antiferromagnetic, while Mn_4 is ferromagnetic. With each Mn atom carrying a magnetic moment of $5\mu_B$ arising from its five $3d$ electrons, Mn_4 carries a giant magnetic moment of $20\mu_B$. This has been demonstrated theoretically in the gas phase[14] and measured by electron spin resonance experiment in a rare gas matrix.[15] Can Mn_4 retain its giant magnetic moment when encapsulated inside an $Al_{12}Au_{20}^{2-}$ cage?

To study the above possibility we considered three different isomers of the neutral $Mn_4@Al_{12}Au_{20}$ cluster. Two starting configurations with T and C_{2v} symmetries were generated from the isomer in Fig. 1(a_4) and a third isomer using the cage structure in Fig. 1(c_4). The optimized structures are given in Fig. 3. We see that the endohedral complexes in Figs. 3(a) and 3(b) are significantly higher in energy than the structure in Fig. 3(c). Spin polarized calculations yielded a

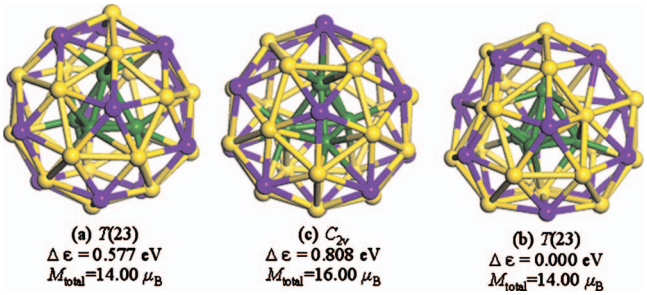

FIG. 3. Optimized structures, relative energy $\Delta\varepsilon$, and total magnetic moment M_{total} of $Mn_4@Al_{12}Au_{20}$ for three isomers. (a) and (b) are generated from isomer A and (c) from isomer C in Fig. 1.

total magnetic moment of the cluster in Fig. 3(c) to be $14\mu_B$ of which $3.718\mu_B$, $3.713\mu_B$, $3.713\mu_B$, and $3.710\mu_B$ reside on each of the Mn atoms. Thus, the Mn atoms are coupled ferromagnetically. In comparison, an isolated Mn_4 cluster has total magnetic moment of $20\mu_B$. Note that the $14\mu_B$ value is obtained by using the *Aufbau* principle where electrons of both spins occupy successive energy levels and the total moment is obtained by integrating the spin density of states. In order to check if there are other spin states close in energy, we carried out a detailed calculation for each possible spin multiplicity ranging from 1 to 21. The relative energies measured with respect to the lowest energy spin state are plotted in Fig. 4(b). These results are compared with the corresponding values in an isolated Mn_4 cluster, which are shown in Fig. 4(a). This analysis shows that an antiferromagnetic state (total spin=0) is the lowest energy state, with the $14\mu_B$ ferromagnetic state lying only 0.09 eV higher in energy. In the antiferromagnetic configuration, the average bond length of Mn_4 endohedral cluster is 2.485 Å, which is significantly

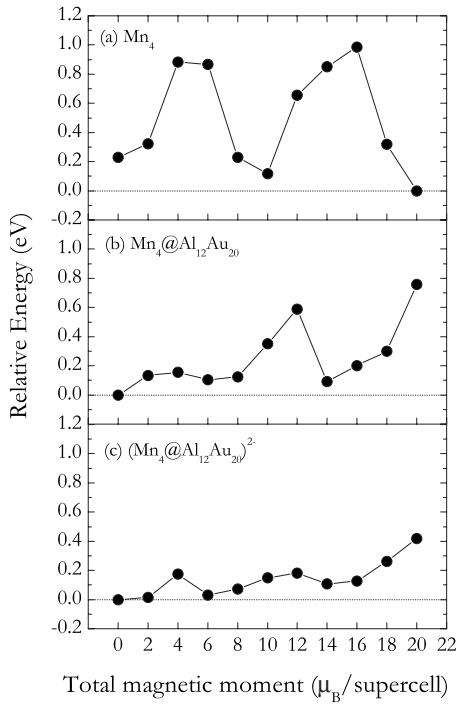

FIG. 4. Relative energies of different magnetic configurations of Mn_4, $Mn_4@Al_{12}Au_{20}$, and $[Mn_4@Al_{12}Au_{20}]^{2-}$ clusters measured with respect to their respective lowest energy configuration.

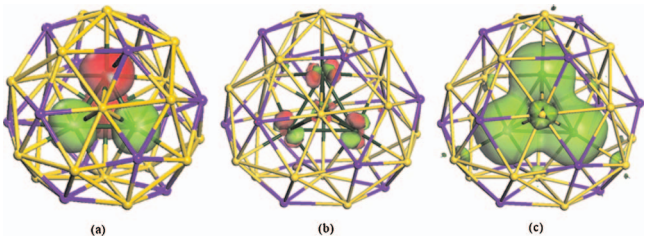

FIG. 5. Isosurfaces of (a) the spin density distribution (0.055 $e/\text{Å}^3$) of $Mn_4@Al_{12}Au_{20}$ cluster with total magnetic moment of $0\mu_B$. (b) The HOMO (0.035 $e/\text{Å}^3$) and (c) the spin density distribution (0.035 $e/\text{Å}^3$) of $Mn_4@Al_{12}Au_{20}^{2-}$ cluster with total magnetic moment of $14\mu_B$.

smaller than corresponding value of 2.717 Å in the isolated Mn_4 cluster. Thus, the onset of antiferromagnetic order in the endohedral complex is due to confinement effects. The spin density distribution is plotted in Fig. 5(a), which clearly shows the antiferromagnetic coupling between the Mn atoms. The binding energy of $Mn_4@Al_{12}Au_{20}$ cluster measured with respect to dissociation into Mn_4 and $Al_{12}Au_{20}$ clusters is 5.74 eV. This large binding energy is particularly interesting since Mn interacts weakly with itself and confirms the stability of the endohedral cluster.

In order to see if the magnetic bistability can be lifted by embedding the Mn_4 cluster inside the $Al_{12}Au_{20}^{2-}$ cluster, we have optimized the geometry of $Mn_4@Al_{12}Au_{20}^{2-}$ cluster by starting with the structure in Fig. 3(c) as the starting configuration, adding two electrons, and calculating the total energies for each spin multiplicity ranging from 1 to 21. Since $Al_{12}Au_{20}^{2-}$ cluster is a closed shell system and hence is expected to interact weakly, we expected that Mn_4 may be able to retain its $20\mu_B$ magnetic moment as in the isolated state. The results in Fig. 4(c) show otherwise. Configurations with $0\mu_B$, $2\mu_B$, and $6\mu_B$ magnetic moments have nearly the same energy, and the $14\mu_B$ configuration lies 0.07 eV above the lowest spin state. For the lowest energy configuration with $0\mu_B$ magnetic moment, the binding energy of $Mn_4@Al_{12}Au_{20}^{2-}$ measured against dissociation into Mn_4 and $Al_{12}Au_{20}^{2-}$ is 5.29 eV. Comparison of results in Figs. 4(a)–4(c) shows that the magnetic moment of the Mn_4 cluster can be altered not only by embedding the cluster inside a metallic cage but also by changing the charge on the cluster. For the $14\mu_B$ configuration of $Mn_4@Al_{12}Au_{20}^{2-}$, the HOMO-LUMO gap is found to be 0.102 eV, indicating that the complex is more metalliclike, as compared to that for $Al_{12}Au_{20}^{2-}$ having the HOMO-LUMO gap of 1.150 eV. The HOMO, as shown in Fig. 5(b), is mainly contributed from the orbitals of encapsulated Mn_4, and similar feature is also found for the LUMO. The spin density distribution shows [see Fig. 5(c)] that the magnetic moment mainly comes from the embedded Mn_4 tetrahedron with small contributions from the neighboring Au atoms due to the spin polarization.

In conclusion we have shown that although the lowest energy structure of $Al_{12}Au_{20}^{2-}$ cluster is a compact one, hollow cage isomers with I_h and T_h symmetries are metastable. This 22 karat hollow golden cage is not only stable against autoelectron detachment and but is also capable of encapsulating a small cluster such as a Mn_4 cluster, which exhibits magnetic bistability with both antiferromagnetic and ferromagnetic states being energetically nearly degenerate. The stability of the dianion cluster suggests that the negative charges can be counterbalanced by incorporating appropriate cations and the resulting ionically bonded complex (e.g., $Cs_2Mn_4@Al_{12}Au_{20}$) can form the building block of a new salt where the magnetic bistability of the anion complex can be manipulated to fabricate new magnetic devices. Experimental verification of our predictions through PES, trapped ion electron diffraction, and infrared spectroscopy is eagerly awaited.

ACKNOWLEDGMENTS

This work was supported by a grant from the Department of Energy.

[1] H. W. Kroto, J. R. Heath, S. C. O'Brien, R. F. Curl, and R. E. Smalley, Nature (London) **318**, 162 (1985).
[2] N. Gonzalez Szwacki, A. Sadrzadeh, and B. I. Yakobson, Phys. Rev. Lett. **98**, 166804 (2007).
[3] I. Boustani, A. Rubio, and J. Alonso, Chem. Phys. Lett. **311**, 21 (1999).
[4] S. Bulusu, X. Li, L.-S. Wang, and X. C. Zeng, Proc. Natl. Acad. Sci. U.S.A. **103**, 8326 (2006).
[5] L. F. Cui, X. Huang, L. M. Wang, D. Y. Zubarev, A. I. Boldyrev, J. Li, and L. S. Wang, J. Am. Chem. Soc. **128**, 8390 (2006).
[6] M. Haruta, Catal. Today **36**, 153 (1997).
[7] Y. Yamamoto, T. Miura, M. Suzuki, N. Kawamura, H. Miyagawa, T. Nakamura, K. Kobayashi, T. Teranishi, and H. Hori, Phys. Rev. Lett. **93**, 116801 (2004).
[8] H. Häkkinen, B. Yoon, U. Landman, X. Li, H.-J. Zhai, and L.-S. Wang, J. Phys. Chem. A **107**, 6168 (2003).
[9] J. Li, X. Li, H.-J. Zhai, and L.-S. Wang, Science **299**, 864 (2003).
[10] V. Kumar, Phys. Rev. B **79**, 085423 (2009).
[11] W. A. de Heer, Rev. Mod. Phys. **65**, 611 (1993).
[12] S. N. Khanna and P. Jena, Phys. Rev. Lett. **69**, 1664 (1992).
[13] M. Ji, X. Gu, X. Li, X. Gong, J. Li, and L.-S. Wang, Angew. Chem., Int. Ed. **44**, 7119 (2005).
[14] S. K. Nayak, B. K. Rao, and P. Jena, J. Phys.: Condens. Matter **10**, 10863 (1998).
[15] C. A. Baumann, R. J. VanZee, S. Bhat, and W. Weltner, Jr., J. Chem. Phys. **78**, 190 (1983).
[16] Y. Wang and J. P. Perdew, Phys. Rev. B **44**, 13298 (1991).
[17] G. Kresse and J. Joubert, Phys. Rev. B **59**, 1758 (1999).
[18] G. Kresse and J. Furthmüller, Phys. Rev. B **54**, 11169 (1996).
[19] S. Nosé, J. Chem. Phys. **81**, 511 (1984).
[20] *Handbook of Chemistry and Physics*, 80th ed., edited by D. R. Lide (CRC, Boca Raton, 2000), pp. 9–52.
[21] *Handbook of Chemistry and Physics*, 80th ed., edited by D. R. Lide (CRC, Boca Raton, 2000), pp. 9–82.
[22] G. W. Ludwig, H. H. Woodbury, and R. O. Carlson, J. Phys. Chem. Solids **8**, 490 (1959).